



## Compton ionization momentum spectrum from neutral hydrogenlike atoms

Dejia Dai  and Libin Fu \**Graduate School, China Academy of Engineering Physics, Beijing 100193, China*

(Received 7 January 2023; revised 13 April 2023; accepted 17 April 2023; published 26 April 2023)

We investigate the ionization momentum spectrum of a bound system composed of two oppositely charged particles, which interact via electromagnetic forces, under nonrelativistic Compton scattering. Our analysis focuses on positronium, a unique system that can be experimentally realized. We find that as the incident photon energy increases, the ionization momentum spectrum of positrons and electrons converges to their respective bound-state momentum distributions. This property distinguishes positronium from the hydrogen atom and can be attributed to the mass ratio  $R_m$  of the two particles in the system. We provide a detailed analysis of the effect of  $R_m$  and demonstrate the existence of hydrogenlike atoms with  $R_m \neq 1$  that exhibit similar behavior in Compton scattering. Such atoms correspond to exotic systems found in nature.

DOI: [10.1103/PhysRevA.107.043118](https://doi.org/10.1103/PhysRevA.107.043118)

## I. INTRODUCTION

X rays are a ubiquitous and powerful tool in modern scientific research, capable of being scattered, absorbed, reflected, and transmitted as they interact with matter. When x rays are scattered, the physical mechanisms involved can be divided into two types depending on whether the photon energy is lost or not. One type is Thomson scattering [1], which is an elastic scattering process, and the other is Compton scattering [2]. Thomson scattering has been widely and effectively utilized in physical structure detection [3,4]. Compton scattering, as an inelastic scattering process, is closely related to the momentum distribution of electrons [5–9] and has thus been applied in many fields, including the detection of the internal structure of atoms and molecules [10,11] and the imaging of ultrafast processes [12–15]. Nevertheless, basic research on Compton scattering is ongoing [16–18].

By utilizing the highly efficient cold target recoil ion momentum spectroscopy technique [19], coincidence experiments on the Compton effect of atoms or molecules are no longer limited to solid targets. A recent study [20] reported a coincidence experiment for helium atoms (gas targets) by detecting electrons and ions in coincidence, thus avoiding the difficulties of measuring scattered photons. This also enables Compton scattering experiments of various gas molecules or atoms. While in the past important studies [7–10] mainly focused on the light-scattering spectrum of atoms, the ionization spectrum of ionized electrons and ions was rarely discussed. Recently, some studies [17,18] have proposed the possibility of using the Compton ionization momentum spectrum to detect the momentum information of electrons in atoms, showing that the ionization momentum spectrum in Compton scattering contains rich information about the structure of atoms. Inspired by these findings, we investigate the Compton ionization spectrum of hydrogenlike atoms in this paper.

The hydrogenlike atom is the simplest bound system caused by electromagnetic interactions, consisting of two charge centers. During Compton scattering, both positive and negative charge centers interact with the electromagnetic field, leading to interference effects whose magnitude depends on the mass ratio  $R_m$  of the positive to negative charge centers. Reference [21] presented the contribution of interference effects to the light-scattering spectrum of positronium and the hydrogen atom. Moreover, a recent work [22] calculated and analyzed the Compton ionization of positronium and hydrogen atoms at incident photon energies below 5 keV and found the resonance effect of the double-differential cross section with respect to positronium.

In this paper we numerically calculate the ionization momentum spectrum of two free particles produced by neutral hydrogenlike atoms in Compton scattering under nonrelativistic limits. We show that when  $R_m = 1$ , the ionization momentum spectrum of two particles approaches the bound-state momentum distribution as the incident photon energy increases. Positronium [23] serves as an example of such a system, and its characteristic lifetime (on the order of nanoseconds) [24] allows for a feasible Compton scattering experiment. Moreover, when  $R_m > 1$ , we observe the same behavior in the momentum spectrum of the particle with greater mass. However, the properties of the momentum spectrum of the other particle depend heavily on  $R_m$ . To further analyze this, we also calculate the energy spectrum of the particle with smaller mass. The results indicate that at higher incident photon energy (greater than or equal to 10 keV), the energy spectrum presents two peaks and there may exist a critical value of  $R_m$ . When  $R_m$  is smaller than this value, the second peak of the energy spectrum decays or even disappears as the incident photon energy increases.

The paper is organized as follows. In Sec. II we describe the calculation process of the ionization momentum spectrum in detail. Our numerical results are presented in Sec. III. We summarize in Sec. IV. Unless stated otherwise, atomic units (a.u.) with  $\hbar = e = 1$  and  $c \approx 137.036$  are employed

\*lbfu@gascaep.ac.cn

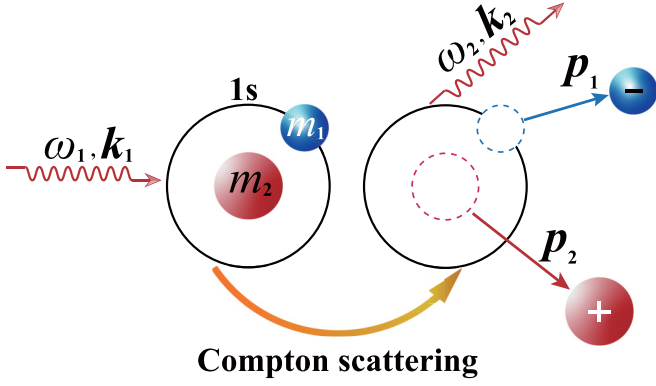


FIG. 1. Schematic of Compton scattering from hydrogenlike atoms. Here  $\mathbf{k}_1$  and  $\mathbf{k}_2$  represent the momentum of the incident and scattered photons, respectively, and  $\mathbf{p}_1$  and  $\mathbf{p}_2$  are the momentum of particles  $m_1$  and  $m_2$  after ionization, respectively.

throughout this paper. Here  $e$  represents the elementary charge and  $c$  is the speed of light.

## II. METHOD

For the two particles constituting the hydrogenlike atom, we denote their masses by  $m_1$  and  $m_2$  (also used as names later in the article), respectively. Without loss of generality, we can set  $m_1 = 1$  a.u. and assume that  $m_2 > m_1$  and both particles carry a unit charge. We now consider the Compton ionization momentum spectrum of  $m_1$  and  $m_2$ ; the corresponding dynamic process is depicted in Fig. 1.

The Hamiltonian of the whole system is written as

$$H = H_0 + H_I, \quad (1)$$

where

$$H_0 = \frac{\mathbf{p}_1^2}{2m_1} + \frac{\mathbf{p}_2^2}{2m_2} + V(\mathbf{r}_1, \mathbf{r}_2) \quad (2)$$

and

$$H_I = \frac{A^2(\mathbf{r}_1, t)}{2m_1} + \frac{A^2(\mathbf{r}_2, t)}{2m_2} + \frac{\mathbf{p}_1 \cdot \mathbf{A}(\mathbf{r}_1, t)}{m_1} - \frac{\mathbf{p}_2 \cdot \mathbf{A}(\mathbf{r}_2, t)}{m_2}. \quad (3)$$

Here  $V(\mathbf{r}_1, \mathbf{r}_2) = -\frac{1}{|\mathbf{r}_1 - \mathbf{r}_2|}$  is the Coulomb interaction energy and

$$A(\mathbf{x}, t) = \sum_{\mathbf{k}, s} g_{\mathbf{k}}(e^{-i\omega t} e^{i\mathbf{k} \cdot \mathbf{x}} \boldsymbol{\epsilon}_{\mathbf{k}, s} a_{\mathbf{k}, s} + \text{H.c.}). \quad (4)$$

In Eq. (4),  $g_{\mathbf{k}} = \sqrt{\frac{2\pi}{\omega V}}$ , with  $V$  the normalized volume of the light field. In addition,  $\omega = c|\mathbf{k}|$ ,  $a_{\mathbf{k}, s}$  is the annihilation operator for photons, and  $\boldsymbol{\epsilon}_{\mathbf{k}, s}$  is the polarization vector of the light field. Since the Coulomb gauge is used,  $s = 1, 2$ .

Let the initial and final states of the whole system be  $\phi_i$  and  $\phi_f$ , respectively. Using the centroid coordinate  $\mathbf{R}$  and the

relative coordinate  $\mathbf{r}$ , we have

$$\begin{aligned} \phi_i &= \frac{1}{\sqrt{V}} \varphi_0(\mathbf{r}) e^{i\mathbf{0} \cdot \mathbf{R}} e^{-i\varepsilon_0 t} \otimes |1_{\mathbf{k}_1}\rangle \otimes |0_{\mathbf{k}_2}\rangle, \\ \phi_f &= \frac{1}{\sqrt{V}} \varphi_p(\mathbf{r}) e^{i\mathbf{P} \cdot \mathbf{R}} e^{-i(E_p + E_p)t} \otimes |0_{\mathbf{k}_1}\rangle \otimes |1_{\mathbf{k}_2}\rangle. \end{aligned} \quad (5)$$

Here

$$\mathbf{r} = \mathbf{r}_1 - \mathbf{r}_2, \quad \mathbf{R} = \frac{m_1 \mathbf{r}_1 + m_2 \mathbf{r}_2}{m_1 + m_2}. \quad (6)$$

In addition,  $\mathbf{P}$  and  $\mathbf{p}$  are the final center-of-mass momentum and relative momentum, respectively, and we assume that the initial center-of-mass momentum is zero. Meanwhile, we also neglect the distribution of the center-of-mass momentum. This is because, in experiments, the target gas is cooled down to temperatures of a only a few kelvin or even below [19] to avoid the momentum fluctuations caused by thermal motion. The expressions for  $E_p$  and  $E_p$  are given by  $E_p = p^2/2\mu$  and  $E_p = P^2/2M$ , respectively, where  $M = m_1 + m_2$  and  $\mu = m_1 m_2 / (m_1 + m_2)$  is the reduced mass. Here  $\varepsilon_0$  is the ground-state energy of the hydrogenlike atom. In addition,  $\varphi_0(\mathbf{r})$  and  $\varphi_p(\mathbf{r})$  are given by

$$\begin{aligned} \varphi_0(\mathbf{r}) &= (\pi a^3)^{-1/2} \exp(-r/a), \\ \varphi_p(\mathbf{r}) &= V^{-1/2} \Gamma(1 + i\eta) e^{\pi\eta/2} e^{i\mathbf{p} \cdot \mathbf{r}} F[-i\eta, 1, -i\mathbf{p} \cdot \mathbf{r}]. \end{aligned} \quad (7)$$

In the above formulas,  $\eta = \mu/p$  and  $F$  is the confluent hypergeometric function.

In our paper we consider only the  $A^2$  approximation [7]. The amplitude for a transition from the initial state to the final state is given by

$$W_{fi} = \int_0^T \langle \phi_f | \frac{1}{2m_1} A^2(\mathbf{r}_1, t) + \frac{1}{2m_2} A^2(\mathbf{r}_2, t) | \phi_i \rangle dt. \quad (8)$$

Thus, we can obtain the total scattering cross section

$$\begin{aligned} \sigma &= \frac{1}{2} \sum_i \sum_f \lim_{T \rightarrow \infty} \frac{V |W_{fi}|^2}{cT} \\ &= G \iiint \frac{1}{\omega_1 \omega_2} (1 + \cos^2 \theta) |M|^2 \\ &\quad \times \delta\left(\omega_1 + \varepsilon_0 - \omega_2 - \frac{\mathbf{p}_1^2}{2m_1} - \frac{\mathbf{p}_2^2}{2m_2}\right) \\ &\quad \times \delta(\mathbf{k}_1 - \mathbf{k}_2 - \mathbf{p}_1 - \mathbf{p}_2) d\mathbf{k}_2 d\mathbf{p}_1 d\mathbf{p}_2. \end{aligned} \quad (9)$$

In Eq. (9),  $\frac{1}{2}$  comes from averaging the photon polarization in the initial state and  $G$  is a constant. In addition,  $\theta$  is the angle between  $\mathbf{k}_1$  and  $\mathbf{k}_2$ , and  $\omega_1 = c|\mathbf{k}_1|$  and  $\omega_2 = c|\mathbf{k}_2|$ . Here we might as well set the  $z$  axis along the direction of  $\mathbf{k}_1$ . Note that  $\mathbf{p} = \frac{1}{M}(m_2 \mathbf{p}_1 - m_1 \mathbf{p}_2)$  and  $\mathbf{P} = \mathbf{p}_1 + \mathbf{p}_2$ . The function  $M$  is given by

$$M = \langle \varphi_p(\mathbf{r}) | \frac{1}{m_1} e^{i(m_2/M)\mathbf{k} \cdot \mathbf{r}} + \frac{1}{m_2} e^{-i(m_1/M)\mathbf{k} \cdot \mathbf{r}} | \varphi_0(\mathbf{r}) \rangle, \quad (10)$$

where  $\mathbf{k} = \mathbf{k}_1 - \mathbf{k}_2$ . According to Ref. [25],

$$\langle \varphi_p(\mathbf{r}) | e^{i\mathbf{k} \cdot \mathbf{r}} | \varphi_0(\mathbf{r}) \rangle = -16\pi \sqrt{\frac{\mu^5}{\pi V}} \Gamma(1 - i\eta) e^{\pi\eta/2} [k^2 - (p + i\mu)^2]^{-1-i\eta} [(k - p)^2 + \mu^2]^{-2+i\eta} \left[ k^2 - (p + i\mu) \frac{\mathbf{p} \cdot \mathbf{k}}{p} \right]. \quad (11)$$

For convenience, let

$$E_f = \frac{p_1^2}{2m_1} + \frac{p_2^2}{2m_2} + \omega_2. \quad (12)$$

We then have

$$c^3 dk_2 = \omega_2^2 \frac{d\omega_2}{dE_f} \sin \theta d\theta d\varphi dE_f, \quad (13)$$

where  $\mathbf{k}_2/|\mathbf{k}_2| = (\sin \theta \cos \varphi, \sin \theta \sin \varphi, \cos \theta)$ . In Eq. (9) we could integrate  $\mathbf{p}_2$  to obtain the conservation of momentum, that is,

$$\mathbf{p}_2 = \mathbf{k}_1 - \mathbf{k}_2 - \mathbf{p}_1. \quad (14)$$

Substituting Eq. (14) into Eq. (12), we have

$$E_f = \frac{p_1^2}{2m_1} + \frac{(\mathbf{k}_1 - \mathbf{k}_2 - \mathbf{p}_1)^2}{2m_2} + \omega_2. \quad (15)$$

Before integrating  $\mathbf{p}_1$ ,  $\theta$ , and  $\varphi$ , they could be treated as constants. Therefore, there are only two variables  $\omega_2$  and  $E_f$  in Eq. (15). By a simple derivative, we can obtain

$$\frac{d\omega_2}{dE_f} = \frac{m_2 c^2}{m_2 c^2 + \omega_2 - \omega_1 \cos \theta + c \mathbf{p}_1 \cdot \mathbf{e}_2}, \quad (16)$$

where  $\mathbf{e}_2 = \mathbf{k}_2/|\mathbf{k}_2|$ .

Finally, the momentum spectrum of the particle  $m_1$  is given by

$$\frac{d^3 \sigma}{dp_{1x} dp_{1y} dp_{1z}} = \iint \frac{\omega_2}{\omega_1} (1 + \cos^2 \theta) \frac{d\omega_2}{dE_f} |M|^2 \sin \theta d\theta d\varphi. \quad (17)$$

In Eq. (17) we have omitted the constant  $G$  because it does not affect the properties of the whole momentum spectrum. Also,  $M$  is just a function of  $\mathbf{p}_1$ ,  $\theta$ , and  $\varphi$ . The conservation of energy can be obtained by integrating  $\omega_2$  in Eq. (9), that is,

$$\omega_1 + \varepsilon_0 = \frac{p_1^2}{2m_1} + \frac{(\mathbf{k}_1 - \mathbf{k}_2 - \mathbf{p}_1)^2}{2m_2} + \omega_2. \quad (18)$$

When  $\mathbf{p}_1$ ,  $\theta$ , and  $\varphi$  are given,  $\omega_2$  is calculated by the equation

$$\begin{aligned} \frac{\omega_2^2}{2m_2 c^2} + \left(1 - \frac{\omega_1 \cos \theta}{m_2 c^2} + \frac{\mathbf{p}_1 \cdot \mathbf{e}_2}{m_2 c}\right) \omega_2 \\ + \frac{(\mathbf{p}_1 - \mathbf{k}_1)^2}{2m_2} + \frac{p_1^2}{2m_1} - \omega_1 - \varepsilon_0 = 0. \end{aligned} \quad (19)$$

In the nonrelativistic case,  $1 - \frac{\omega_1 \cos \theta}{m_2 c^2} + \frac{\mathbf{p}_1 \cdot \mathbf{e}_2}{m_2 c} > 0$  and  $\frac{(\mathbf{p}_1 - \mathbf{k}_1)^2}{2m_2} + \frac{p_1^2}{2m_1} - \omega_1 - \varepsilon_0 < 0$ , so the solution of Eq. (19) is unique. Similarly, the momentum spectrum  $d^3 \sigma / dp_{2x} dp_{2y} dp_{2z}$  of the particle  $m_2$  can also be calculated.

### III. NUMERICAL RESULTS

Let us introduce a dimensionless parameter  $R_m = m_2/m_1$ . In this section we analyze and discuss the ionization momentum spectrum or energy spectrum corresponding to different  $R_m$ . The conclusions obtained for the same  $R_m$  are universal, regardless of the specific values of  $m_1$  and  $m_2$ . As the integral in Eq. (17) does not have an analytic expression, we can

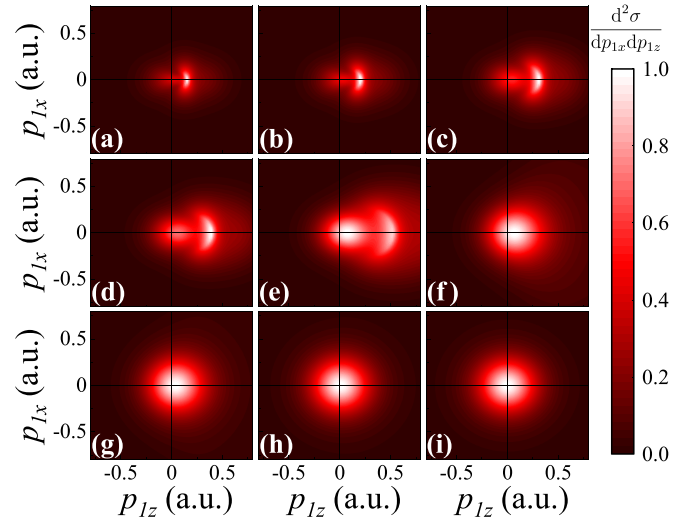


FIG. 2. Ionization momentum spectrum  $d^2 \sigma / dp_{1x} dp_{1z}$  from positronium, with incident photon energy  $\omega_1$  of (a) 0.6, (b) 0.8, (c) 1.2, (d) 1.5, (e) 2, (f) 5, (g) 10, and (h) 50 keV. (i) Momentum distribution of the electron or positron in the ground state of positronium in the  $x$ - $z$  plane.

only handle it numerically. The  $\varphi_0(\mathbf{r})$  is independent of spatial orientation, so we will just focus on the momentum spectrum in the  $x$ - $z$  plane. Furthermore, the numerical results presented in this section have been normalized.

#### A. Positronium and $R_m = 1$

Positronium is a system composed of an electron and a positron. It is evident that the ionization momentum spectrum of the electron is identical to that of the positron. In Fig. 2 we present the ionization momentum spectrum  $d^2 \sigma / dp_{1x} dp_{1z}$  from positronium corresponding to various incident photon energies. For positronium, its ionization threshold [20]  $\omega_1 \approx 0.75$  keV. First, we observe that when  $\omega_1 = 0.6$  keV, there is only one island structure. The island is the result of the forward transfer of photon momentum. In contrast to helium atoms with two electrons, however, there is no recoil island [20] observed near the threshold from positronium. This indicates that the recoil island of the momentum distribution of the  $\text{He}^+$  ion in Ref. [20] is primarily caused by the repulsion between two electrons.

Next, as depicted in Figs. 2(a)–2(h), a second island emerges near the origin and gradually becomes stronger and closer to the origin as  $\omega_1$  increases. Meanwhile, the first island to form strengthens, then weakens, and eventually disappears as it moves to the right. In fact, these phenomena could be explained qualitatively from Eq. (10). Specifically, it can be considered that the term  $e^{i(m_2/M)\mathbf{k} \cdot \mathbf{r}}/m_1$  controls the first island and the other term  $e^{-i(m_1/M)\mathbf{k} \cdot \mathbf{r}}/m_2$  shows momentum transfer as  $-\mathbf{k}$ . Therefore, the latter would weaken the strength of the first island and affect the formation of the second island. In the case of positronium, for incident photon energies that are large, the interference effect between the former and the latter disappears and their contributions to the light-scattering spectrum become identical [21]. As a result, in Fig. 2(h),

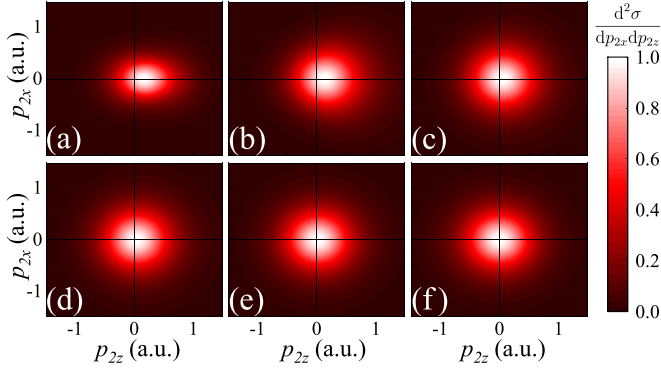


FIG. 3. Ionization momentum spectrum  $d^2\sigma/dp_{2x}dp_{2z}$  from hydrogen atoms, with incident photon energy  $\omega_1$  of (a) 1.5, (b) 5, (c) 15, (d) 20, and (e) 40 keV. (f) Momentum distribution of  $H^+$  ions in the ground state of the hydrogen atom.

only one island remains, which is nearly symmetric about the  $x$  axis.

In addition, it can be observed that  $d^2\sigma/dp_{1x}dp_{1z}$  exhibits asymptotic behavior and tends to stabilize as  $\omega_1$  increases. For comparison, the momentum distribution of the electron or positron in the ground state of positronium in the  $x$ - $z$  plane is shown in Fig. 2(i). By comparing Fig. 2(i) with Fig. 2(h), it can be clearly seen that  $d^2\sigma/dp_{1x}dp_{1z}$  is very close to the bound-state momentum distribution when  $\omega_1 = 50$  keV. It is as if the electron and positron in the positronium instantaneously lose their interaction under the impact of ultrahigh-energy photons and move separately in free motion. It is worth mentioning that we have previously assumed that the initial center-of-mass momentum is  $\mathbf{0}$ , i.e.,  $\mathbf{p}_1 = -\mathbf{p}_2$ . Thus,  $\mathbf{p} = \mathbf{p}_1 = -\mathbf{p}_2$  and the Fourier transform of  $\varphi_0(\mathbf{r})$  is just the momentum distribution of the electron or positron in the ground state of positronium. Since  $d^3\sigma/dp_{1x}dp_{1y}dp_{1z}$  is rotationally symmetric about the  $z$  axis, we can conclude that for  $R_m = 1$ ,  $d^3\sigma/dp_{1x}dp_{1y}dp_{1z}$  will tend to be the initial-state momentum distribution when  $\omega_1$  is large.

### B. $R_m > 1$

As a typical example corresponding to  $R_m > 1$ , the momentum spectrum of  $H^+$  ions from hydrogen atoms ( $R_m = 1836$ ) via Compton scattering is illustrated in Fig. 3. Upon comparing Fig. 3(e) with Fig. 3(f), it is apparent that  $d^2\sigma/dp_{2x}dp_{2z}$  closely resembles the momentum distribution of  $H^+$  ions in the ground state of the hydrogen atom at  $\omega_1 = 40$  keV. A similar phenomenon was also recently reported in an experimental study on helium atoms [16] and it reflects the validity of the impulse approximation [7]. In other words, when the incident photon energy is very high, the bound electrons in the atom are quickly stripped, so the momentum distribution of the atomic nucleus remains unaffected. Next we further calculate  $d^2\sigma/dp_{2x}dp_{2z}$  for various  $R_m$  values. Similar to positronium, interesting phenomena for  $d^2\sigma/dp_{2x}dp_{2z}$  arise as  $\omega_1$  varies. However, we will not present these details here, but rather focus on whether the asymptotic behavior of  $d^2\sigma/dp_{2x}dp_{2z}$  mentioned earlier is affected by  $R_m$ . As shown in Fig. 4, when  $\omega_1 = 50$  keV, the  $d^2\sigma/dp_{2x}dp_{2z}$  for each  $R_m$  tends to their corresponding

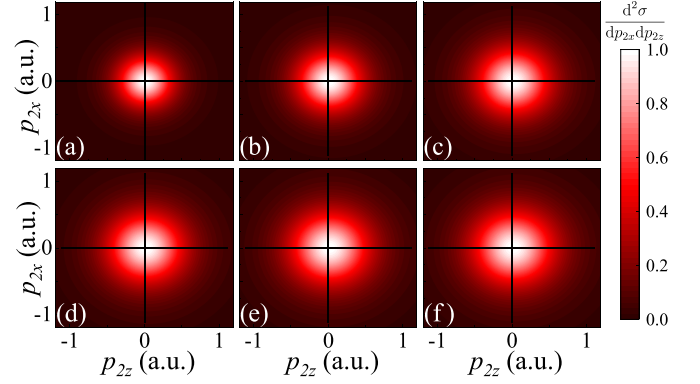


FIG. 4. Ionization momentum spectrum  $d^2\sigma/dp_{2x}dp_{2z}$  from hydrogenlike atoms at  $\omega_1 = 50$  keV, with a mass ratio  $R_m$  of (a) 2, (b) 4, (c) 8, (d) 13, (e) 30, and (f) 206.

bound-state momentum distribution. This indicates that the asymptotic property of  $d^2\sigma/dp_{2x}dp_{2z}$  is independent of  $R_m$  for hydrogenlike atoms.

However, the ionization properties of particle  $m_1$  are distinct. From the aforementioned discussion, we already established that the ionization momentum spectrum of particle  $m_2$  is very close to its bound-state momentum distribution when  $\omega_1$  is large. This naturally raises the question of whether the ionization spectrum of particle  $m_1$  exhibits similar regularity. For convenience, we calculate the ionization energy spectroscopy of particle  $m_1$  by averaging Eq. (17) over the directions of  $\mathbf{p}_1$ , as follows:

$$\frac{d\sigma}{dE_1} = \iint \frac{d^3\sigma}{dp_{1x}dp_{1y}dp_{1z}} \sqrt{E_1} d\Omega. \quad (20)$$

Here  $E_1 = p_1^2/2m_1$  and  $\Omega$  denotes the solid angle corresponding to  $\mathbf{p}_1$ . The numerical results are presented in Figs. 5 and 6, where  $d\sigma/dE_1$  has been replaced by the normalized

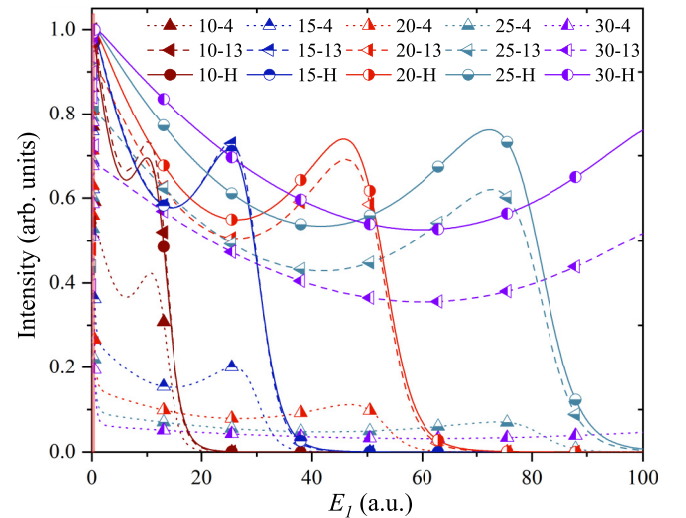


FIG. 5. Ionization energy spectroscopy of the particle  $m_1$  for hydrogenlike atoms. The form  $x$ - $y$  in the legend means that the incident photon energy is  $x$  keV and  $y$  is the value of  $R_m$ . The symbol H represents the hydrogen atom and its corresponding  $R_m = 1836$ .



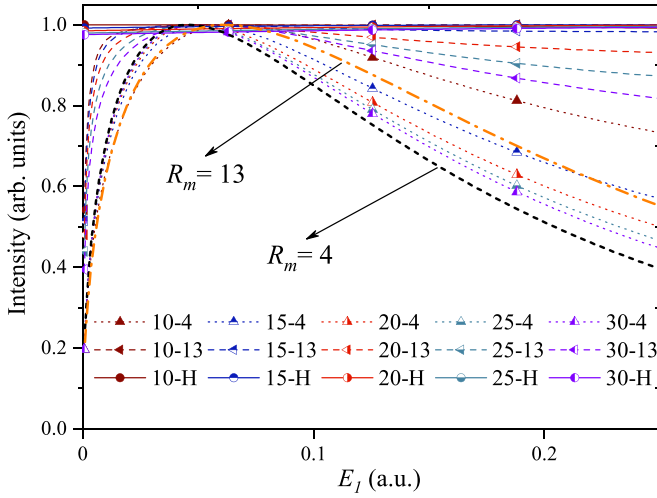


FIG. 6. Partially enlarged view of Fig. 5. Further, as shown by the orange dash-dotted line and the black dashed line in the figure, we also added the bound-state energy spectroscopy of the particle  $m_1$  corresponding to  $R_m = 13$  and 4, respectively.

intensity. It can be observed that, for  $\omega_1 \geq 10$  keV, there are two peaks in the ionization energy spectroscopy of the particle  $m_1$  wherein the first peak is located closer to the origin and the second peak moves to the right as  $\omega_1$  increases. However, some behaviors of the two peaks are essentially different due to the variation in  $R_m$ . For example, the intensity of the second peak corresponding to the hydrogen atom increases with  $\omega_1$ , but the opposite trend is observed for  $R_m = 4$  and 13. Notably, the second peak associated with  $R_m = 4$  is almost disappearing in the current range of data in Fig. 5. Although not all the ionization energy spectroscopy results corresponding to  $R_m$  are presented in this paper, it is evident from Fig. 5 that a critical value of  $R_m$  exists around 13. When  $R_m$  is less than this critical value, the intensity of the second peak decreases with increasing  $\omega_1$ ; otherwise the opposite occurs. As another example, it can be observed from Fig. 6 that the first peaks corresponding to  $R_m = 4$  and 13 gradually approach their respective bound-state energy spectroscopy of particle  $m_1$  as  $\omega_1$  increases. This phenomenon is particularly prominent for  $R_m = 4$ . Also, combined with the properties of the second peak just discussed, it can be inferred that the energy or momentum spectrum of particle  $m_1$  corresponding to  $R_m = 4$  will also tend to the bound-state distribution with  $\omega_1$  increasing. This also implies the existence of hydrogenlike atoms with  $R_m \neq 1$ , which consist of two particles whose ionization momentum spectrum in Compton scattering will be very close to their respective bound-state momentum distributions when the incident photon energy is large. This finding is surprising. In fact, such atoms are found in nature, such as kaonic hydrogen, which is a bound system composed of a negative kaon ( $K^-$ ) and a proton. The decay lifetime of  $K^-$  is about  $1.2 \times 10^{-8}$  s and its rest mass is about 967 times that of the electron. Kaonic hydrogen corresponds to  $R_m \approx 1.9$ , which is less than 4. Obviously, according to our analysis in this paper, kaonic hydrogen is such a system that fits the

criteria. Similar exotic atoms [26,27] also include  $\pi K$  atoms ( $R_m \approx 3.5$ ), pionic hydrogen ( $R_m \approx 6.7$ ), muonic hydrogen ( $R_m \approx 8.9$ ), etc.

It is intriguing to note that kaonic hydrogen, with its simple structure, serves as an excellent experimental subject for probing the strong interaction [26]. We imagine that if the bound-state momentum distribution of charged particles in kaonic hydrogen can be measured directly, the information on strong interaction could be inferred. Our discussion and analysis suggest that Compton scattering could be a viable method for such measurements. This can yet be regarded as a different way to explore the strong interaction. However, it should be noted that the strong interaction that is unknown has not been taken into account in our calculations. In fact, in kaonic hydrogen, the strong interaction shows a repulsive effect and the electromagnetic interaction still dominates. More importantly, the strong interaction affects the internal potential energy  $V(\mathbf{r}_1, \mathbf{r}_2)$  between the  $K^-$  and the proton rather than the interaction Hamiltonian  $H_I$ . Therefore, we have reasons to believe that the conclusions predicted in this paper still hold true for real kaonic hydrogen. Nevertheless, there may still be a long way to go before Compton scattering experiments can be realized on exotic atoms. For instance, it is very challenging to efficiently form exotic atoms [26]. Furthermore, the lifetime of exotic atoms and their constituent mesons is quite limited and the crucial problem of how to measure the momentum of ionized fragments within this limited time also needs to be solved.

#### IV. CONCLUSION

In summary, our investigation focused on the ionization momentum spectrum generated by Compton scattering from neutral hydrogenlike atoms in the nonrelativistic case. By conducting meticulous numerical calculations, we discussed in detail the ionization momentum spectrum of positronium, revealing a noteworthy phenomenon wherein the momentum spectrum of electrons and positrons will tend to their respective bound-state momentum distributions when subjected to high-energy photons. We also examined the impact of the mass ratio  $R_m$  between two particles in hydrogenlike atoms, establishing that the asymptotic property of  $d^2\sigma/dp_{2x}dp_{2z}$  is independent of  $R_m$ . Furthermore, the ionization energy spectroscopy of the less massive particle  $m_1$  was calculated, and it has two peaks. Our analysis indicates that there is a critical value of  $R_m$  that governs the properties of these two peaks. Finally, we also found that there are real hydrogenlike atoms with  $R_m \neq 1$  in nature, which consist of two particles whose ionization momentum spectrum in Compton scattering will be very close to their respective bound-state momentum distributions as  $\omega_1$  increases. This finding may be useful in studying the strong interaction.

#### ACKNOWLEDGMENTS

This work was supported by the National Natural Science Foundation of China (Grants No. 12088101 and No. U1930403) and Science Challenge Project (Grant No. TZ2018005).

- [1] J. J. Thomson, On electrical oscillations and the effects produced by the motion of an electrified sphere, *Proc. London Math. Soc.* **s1-15**, 197 (1883).
- [2] A. H. Compton, The spectrum of scattered x-rays, *Phys. Rev.* **22**, 409 (1923).
- [3] M. F. C. Ladd and R. A. Palmer, *Structure Determination by X-Ray Crystallography* (Springer, Berlin, 1977), Vol. 233.
- [4] S. H. Glenzer and R. Redmer, X-ray Thomson scattering in high energy density plasmas, *Rev. Mod. Phys.* **81**, 1625 (2009).
- [5] J. W. M. Du Mond, Compton modified line structure and its relation to the electron theory of solid bodies, *Phys. Rev.* **33**, 643 (1929).
- [6] P. M. Platzman and N. Tzoar, X-ray scattering from an electron gas, *Phys. Rev.* **139**, A410 (1965).
- [7] P. Eisenberger and P. M. Platzman, Compton scattering of x rays from bound electrons, *Phys. Rev. A* **2**, 415 (1970).
- [8] P. Eisenberger, Electron momentum density of He and H<sub>2</sub>; Compton x-ray scattering, *Phys. Rev. A* **2**, 1678 (1970).
- [9] M. Jain and N. Tzoar, Compton scattering in the presence of coherent electromagnetic radiation, *Phys. Rev. A* **18**, 538 (1978).
- [10] M. J. Cooper, Compton scattering and electron momentum determination, *Rep. Prog. Phys.* **48**, 415 (1985).
- [11] J. M. Slowik, S.-K. Son, G. Dixit, Z. Jurek, and R. Santra, Incoherent x-ray scattering in single molecule imaging, *New J. Phys.* **16**, 073042 (2014).
- [12] G. Dixit, O. Vendrell, and R. Santra, Imaging electronic quantum motion with light, *Proc. Natl. Acad. Sci. USA* **109**, 11636 (2012).
- [13] G. Dixit, J. M. Slowik, and R. Santra, Proposed Imaging of the Ultrafast Electronic Motion in Samples using X-Ray Phase Contrast, *Phys. Rev. Lett.* **110**, 137403 (2013).
- [14] G. Dixit, J. M. Slowik, and R. Santra, Theory of time-resolved nonresonant x-ray scattering for imaging ultrafast coherent electron motion, *Phys. Rev. A* **89**, 043409 (2014).
- [15] G. Dixit and R. Santra, Time-resolved ultrafast x-ray scattering from an incoherent electronic mixture, *Phys. Rev. A* **96**, 053413 (2017).
- [16] M. Kircher, F. Trinter, S. Grundmann *et al.*, Ion and Electron Momentum Distributions from Single and Double Ionization of Helium Induced by Compton Scattering, *Phys. Rev. Lett.* **128**, 053001 (2022).
- [17] O. Chuluunbaatar, S. Houamer, Y. V. Popov, I. P. Volobuev, M. Kircher, and R. Dörner, Compton ionization of atoms as a method of dynamical spectroscopy, *J. Quant. Spectrosc. Radiat. Transfer* **272**, 107820 (2021).
- [18] O. Chuluunbaatar, S. Houamer, Y. Popov, I. P. Volobuev, M. Kircher, and R. Dörner, Compton double ionization of the helium atom: Can it be a method of dynamical spectroscopy of ground state electron correlation? *J. Quant. Spectrosc. Radiat. Transfer* **278**, 108020 (2022).
- [19] J. Ullrich, R. Moshhammer, A. Dorn, R. Dörner, L. P. H. Schmidt, and H. Schmidt-Böcking, Recoil-ion and electron momentum spectroscopy: Reaction-microscopes, *Rep. Prog. Phys.* **66**, 1463 (2003).
- [20] M. Kircher, F. Trinter, S. Grundmann *et al.*, Kinematically complete experimental study of Compton scattering at helium atoms near the threshold, *Nat. Phys.* **16**, 756 (2020).
- [21] Z. Kaliman, K. Pisk, and R. H. Pratt, Compton scattering from positronium and validity of the impulse approximation, *Phys. Rev. A* **83**, 053406 (2011).
- [22] I. Stepantsov, I. Volobuev, and Y. Popov, Comparative analysis of the Compton ionization of hydrogen and positronium, *Eur. Phys. J. D* **76**, 30 (2022).
- [23] D. B. Cassidy, Experimental progress in positronium laser physics, *Eur. Phys. J. D* **72**, 53 (2018).
- [24] M. A. Strosio, Positronium: A review of the theory, *Phys. Rep.* **22**, 215 (1975).
- [25] S. Houamer, O. Chuluunbaatar, Volobuev, I. P. Volobuev, and Y. V. Popov, Compton ionization of hydrogen atom near threshold by photons in the energy range of a few keV: Nonrelativistic approach, *Eur. Phys. J. D* **74**, 81 (2020).
- [26] C. Curceanu, C. Guaraldo, M. Iliescu *et al.*, The modern era of light kaonic atom experiments, *Rev. Mod. Phys.* **91**, 025006 (2019).
- [27] B. Adeva *et al.*, Observation of  $\pi^- K^+$  and  $\pi^+ K^-$  Atoms, *Phys. Rev. Lett.* **117**, 112001 (2016).